General Disclaimer

One or more of the Following Statements may affect this Document

- This document has been reproduced from the best copy furnished by the organizational source. It is being released in the interest of making available as much information as possible.

- This document may contain data, which exceeds the sheet parameters. It was furnished in this condition by the organizational source and is the best copy available.

- This document may contain tone-on-tone or color graphs, charts and/or pictures, which have been reproduced in black and white.

- This document is paginated as submitted by the original source.

- Portions of this document are not fully legible due to the historical nature of some of the material. However, it is the best reproduction available from the original submission.

TABLE OF CONTENTS

	Page
LIST OF ILLUSTRATIONS	i
ABSTRACT	1
ACKNOWLEDGEMENTS	2
LIST OF SYMBOLS	3
1. INTRODUCTION	4
1.1 State of Art of Helicopter Rotor Impulsive Noise	4
1.2 Acoustical Triangulation	8
2. IMPULSIVE NOISE TRIANGULATION TECHNIQUES	12
2.1 Formulation of Triangulation Equations	12
2.2 Numerical Techniques	16
2.3 Sensitivity to Experimental Errors	17
3. APPLICATIONS TO FULL SCALE NOISE DATA	19
3.1 Rotor Noise Data	19
3.2 Noise Source Locations and Noise Mechanisms	20
4. CONCLUSIONS	25
REFERENCES	27
TABLES	
ILLUSTRATIONS	

ABSTRACT

The state of the art of helicopter rotor impulsive noise is reviewed. A triangulation technique for locating impulsive noise sources is developed using once-per-rev index signals as time references. A computer program (INSL) has been written implementing this technique. Applying triangulation to the full-scale UH-1 noise data of NASA/Ames Research Center 40- by 80-Foot Wind Tunnel, three different noise sources are found on the rotor disk. The primary sources of thickness noise are in the second quadrant and on the advancing side of rotor disk. Two aerodynamic sources due to blade/vortex interaction are found in the first quadrant.

ACKNOWLEDGEMENTS

The author wishes to express his appreciation to Mr. John P. Rabbott, Mr. James C. Biggers, and Mr. Robert H. Stroub for their valuable suggestions and help during the course of this effort.

The work reported here was sponsored by NASA Ames Research Center, under NASA Grant NSG 2095. The technical monitor is Mr. John P. Rabbott, Large Scale Aerodynamics Branch, NASA Ames Research Center.

LIST OF SYMBOLS

a_o	rotor coning angle
a_{1_s}	rotor longitudinal flapping coefficient
b_{1_s}	rotor lateral flapping coefficient
C	speed of sound in still air
C_{eff}	effective speed of sound
g	length of shaft
R	distance between source and observer
r	radial distance of source from rotor hub
t	observer time ($t = \zeta + R/C$)
t_1	time taken for sound traveling from source to observer
T	time between acoustical signature and $\psi = 0$ index
TEM	tunnel temperature
U_∞	free stream velocity
x,y,z	source location (see Figure 1 for coordinate system)
x_1, y_1, z_1	observer location (see Figure 1)
α_S	angle of rotor shaft from vertical, positive shaft tilted aft
α_{TPP}	angle of rotor tip path plane from horizontal, positive tip path plane tilted aft
β	rotor flapping angle with respect to rotor shaft plane
β_0	rotor flapping angle with respect to horizontal
ζ	source time
Ω	rotor rotational velocity
ψ	azimuthal angle. $\psi = 0$ along the negative X- axis

1. Introduction

One of the most serious problems in the development of a helicopter transportation system for civilian or military requirements is the noise generated by these vehicles due to aerodynamic mechanisms inherent in their design. For a typical helicopter, aerodynamic noise is produced by the main rotor, the tail rotor, and the engine. According to Cox[1] (1973), the aerodynamic noise from main rotors can be classified into two main categories: rotational (harmonic) noise and broadband noise. The aerodynamic sources of rotational noise are mean lift and drag force, harmonic force fluctuations, and blade thickness. The sources of broadband noise are random force fluctuations, and wake self-noise. A prominent and impulsive sound occurs when a helicopter operates in certain conditions. This impulsive sound is usually called blade slap or impulsive noise. Impulsive noise belongs to the rotational noise category, but it is usually distinguished from rotational noise. When impulsive noise occurs, it dominates all other noise sources.

At low tip speed, the mechanism of impulsive noise is blade-vortex interaction. For high tip Mach numbers, the impulsive noise could be due to one or a combination of the following mechanisms: (1) blade-vortex interaction, (2) compressibility, and (3) thickness.

1.1 State of the Art on Rotor Impulsive Noise

Interactions of the blade with the vortex wake occur to varying degree throughout the normal flight envelope of all helicopters. A blade that passes close to a wake vortex filament experiences a rapid

change in angle of attack. This causes a localized impulsive aerodynamic loading which occurs periodically and results in sound radiation. It is highly probable that stall and local transonic or supersonic flow occur simultaneously in the blade-vortex interaction as indicated by Ham[2] (1974). The primary parameters affecting blade-vortex interaction include strength and size of the vortex filament, vertical spacing between the blade and filament, and relative alignment of the filament with the blade.

Widnall[3] (1971) has derived the expressions for the frequency spectrum, directivity factor, total sound pressure level and waveform of the noise radiated by blade-vortex interaction which occurs near the middle portion of the blade. The aerodynamic modeling is limited to subsonic flow and a two-dimensional blade. This model is suitable for the type of blade-vortex interaction which most likely occurs for tandom rotors. Later, Filotas[4] (1973) obtained similar results.

The blade-vortex interaction of the single rotor is most likely to occur at blade tip region. In this case, the three-dimensional aerodynamic model should be used. Chu and Widnall[5] (1974) developed an unsteady three-dimensional lifting surface theory for the calculation of the unsteady airloads on the helicopter rotor blade due to interaction with a vortex near the tip region. Currently, Widnall is modifying this lifting surface theory to calculate the noise radiation due to blade-vortex interaction at tip region.

All rotors are influenced to some degree by effects of compressibility, the degree being a function of the rotor tip speed, forward speed, and airfoil characteristics. As the advancing blade of main rotors enters the compressible flow region, the blade's outboard aerodynamic loading varies rapidly and results in intense sound radiation. Arndt and Borgman[6] (1970) indicated that the drag divergence and thickness effect are responsible for noise radiation, when the rotor is operating at high advancing tip Mach numbers.

Lyon[7] (1971) demonstrates that when an airfoil of finite thickness changes its forward speed relative to the fluid in an unsteady manner (as does a rotating blade in a forward flight), impulsive noise is generated even though the flow speed is less than sonic everywhere (but a high tip Mach number). Lyon, Mark, and Pyle[8] (1971) conducted a theoretical study on the rotor tip sound radiation due to lift and thickness effects. A computational algorithm was developed for the synthesis of tip shapes that cause minimum thickness radiation in specific frequency bands.

Ffowcs Williams and Hawkings[9] (1969) extended the fundamental aerodynamic sound theories of Lighthill[10] (1952) and Curl[11] (1955) to include the effect of a surface in arbitrary motion. The Kirchhoff description of a homogeneous sound field in terms of surface boundary conditions was generalized to include arbitrary motion. The surface is replaced by a discontinuity in the flow field, around which the motion of the fluid medium is assumed to be known. From the equations

of generalized mass and momentum, a wave equation is obtained which includes Lighthill's equation[10] (1952) as a special case. Ffowcs Williams and Hawkings then proceed to solve this equation in several equivalent forms by a four-dimensional generalized function approach (time being taken as the fourth dimension). Their formulation laid the framework of study the sound field of a surface moving at high speed.

Farassat, Pegg, and Hilton[12] (1975) studied the thickness noise of helicopter rotors at high tip speed. Based on Ffowcs Williams and Hawkings' formulation[9] (1969) and a collapsing sphere method, they solved the wave equation and obtained a solution, which is not restricted to either the compactness or the far-field assumption, for the sound pressure in terms of blade thickness distribution. The thickness noise was found to be directional with peak pressure in the rotor plane towards the forward direction.

The earliest experimental data on the acoustic signature due to blade-vortex interaction was obtained by Riedel and Schairer[13] (1970) and Surrendriah[14] (1970). Widnall, Chu, and Lee[15] (1971) measured the noise radiation due to the interaction of a blade with a straight vortex in an open jet wind tunnel and the results compared favorably with theoretical predictions. Bauch and Schlegel[16] (1971) measured the impulsive noise in flight, and related it to blade-vortex interaction, when the helicopter is in hovering mode. Widnall, Lee, and Bauer[17] (1972) studied the forward flight effect on helicopter rotor

impulsive noise using a model rotor system in an anechoic wind tunnel. Both waveform and spectrum changes due to forward flight effect were studied. Charles[18] (1975) measured helicopter impulsive noise in partial-power descent using a microphone array mounted external to the vehicle. He indicated that shock formation and stall may be responsible for intense slap noise. Schmitz and Boxwell[19] (1976) developed an in-flight station-keeping technique to collect acoustic data. The in-flight data agree reasonably well with 1/7-scale model data measured in a wind tunnel[20]. To study the effects of blade tip shapes and performance conditions over a wide range, full scale experiments were conducted in the 40- by 80-Foot Wind Tunnel at NASA/Ames Research Center. Although these noise data were taken in a hard-walled wind tunnel, they are useful for studying impulsive noise mechanisms and accessing the effects of design changes. The effects of reflections are minimized because the large size of the wind tunnel results in a large delay of the reflections. Thus, the impulsive acoustical signals are not overlapped by reflections. This makes it possible to identify and separate the impulsive signals and their reflections.

1.2 Acoustical Triangulation

High speed rotor impulsive noise can be due to blade-vortex interaction, compressibility effects or thickness effects. Depending on the rotor operating conditions, any or all of these noise mechanisms can generate impulsive noise. The impulsive noise generated by different

mechanisms has different characteristics, including directivity and dependence upon rotor performance. Because of different noise directivity, the impulsive noise observed at different locations may come from different source locations. The knowledge of the source location on the rotor disc can help us to identify and understand the noise mechanism. Consequently, design changes can be made to reduce rotor noise.

Charles[18] (1975) developed a triangulation technique to locate noise sources using a microphone array mounted external to a helicopter. At least four microphone measurements are required if no assumption on source location is made. Four microphone measurements give three independent equations in terms of source location (x,y,z). Each equation is obtained by the difference of arrival time of an acoustical pulse as measured by the microphones. If the noise source was assumed to be on rotor disc (a reasonable assumption), at least three microphone measurements were required. Two equations in terms of (r,ψ) were then obtained to locate the noise source, where r and ψ are the radial and azimuthal location respectively.

There are some disadvantages of the microphone array methods: (i) the three (or two) equations are obtained by the difference of arrival time between microphones, and this time difference is usually very small. A small error on microphone locations can cause a large error in time difference, and therefore source location; (ii) four

(or three) microphones must measure the acoustic radiation from the same source. There are several sources on the rotor disc which can generate impulsive noise, and the impulsive noise is usually quite directional. The microphones must then be arranged so close to each other that they measure the same source. Physically, the noise source location is determined by the intersection of three surfaces. Each surface is determined by source-to-microphone time. When the microphones are close to each other, the intersection is shallow. Consequnetly, a small error on source-to-microphone time will result in a large error in source location; and (iii) the above two disadvantages are problems of accuracy only. Conceptually, very carefully measurements can improve the accuracy, although there may be some difficulties in practice. However, the most severe disadvantage of the microphone array is its incapability of determining the source location of thickness noise which is dominant in the acoustical field in front of a high speed rotor. Unlike the impulsive noise due to blade-vortex interaction or compressibility effect (drag divergence), thickness noise is the result of accumulated acoustic waves which are generated from different portions of rotor but reach a microphone at the same time. The thickness noise measured at different locations are generated from different regions on the disc. The method of the microphone array only works when each microphone is measuring the acoustical signatures coming from the same source. Therefore, the microphone array cannot be applied to thickness noise.

To avoid the disadvantages mentioned above, a triangulation method of using a 1/rev "blip" was developed. The 1/rev "blip" serves as a timing mark. It is generated when a rotor blade is at a specified azimuth (usually directly downstream). The time for an acoustical pulse to reach a microphone is measured relative to the 1/rev "blip." The rotor blade azimuthal location where an acoustical wave is generated can then be determined relative to the 1/rev blip. Two microphones (with the assumption of source being on rotor disc) are all we need. Each microphone determines a source line on rotor disc, and the intersection of two source lines is the source location. For thickness noise, only one microphone is required. This microphone will determine a source line on which the noise source lies. Physically, this source line is the intersecting loci of the rotor blade and a "collapsing sphere" which is determined by $\zeta - t + r/c = 0$, where ζ, t are source time and observer time, respectively. r is the distance between source and observer, and c is the speed of sound. Acoustical waves, which are generated along the source line at different times due to blade thickness effect, will reach the observer at the same time.

The triangulation technique presented in this report was developed for rotor noise measured in the wind tunnel. The effects of tunnel air speed and temperature are taken into account. Both rotor shaft tilt and blade flapping are included in the mathematical formulation. A computer program has been written for numerical calculation. The triangulation technique is applied herein to rotor noise data measured in the 40- by 80-Foot Wind Tunnel, NASA Ames Research Center.

2. Impulsive Noise Triangulation Techniques

2.1 Formulation of Triangulation Equation

Figure 1 shows the coordinate system used in the development of triangulation technique. X-axis is pointing upstream direction of wind tunnel. Y-axis is pointing rotor advancing side. Z-axis is pointing vertically down. The rotor hub is at point A. Points S and P are source location and microphone location, respectively. The source S is assumed to be on the rotor blade.

The flapping angle β with respect to rotor shaft plane (plane normal to rotor shaft) is

$$\beta = a_0 - a_{1S} \cos \psi - b_{1S} \sin \psi \tag{1}$$

where

a_0 is the coning angle

a_{1S} is the longitudinal flapping (cos) coefficient

b_{1S} is the lateral flapping (sin) coefficient

$\psi = 0$ along the negative X-axis

The angle β_0 between horizontal plane and blade is

$$\beta_0 = \beta - \alpha_s \cos \psi \tag{2}$$

Substituting eq (1) into eq (2), we have

$$\begin{aligned} \beta_0 &= a_o - (a_{1S} + \alpha_S) \cos \psi - b_{1S} \sin \psi \\ &= a_0 - \alpha_{TPP} \cos \psi - b_{1S} \sin \psi \end{aligned} \tag{3}$$

From Figure 1(a), we have

$$\vec{OS} = \vec{OA} + \vec{AS}$$

$$\vec{OA} = (-g \sin \alpha_S,\ 0,\ -g \cos \alpha_S)$$

$$\vec{AS} = (-r \cos \psi \cos \beta_0,\ r \sin \psi \cos \beta_0,\ -r \sin \beta_0)$$

Therefore,

$$\vec{OS} = (-g \sin \alpha_S - r \cos \psi \cos \beta_0,\ r \sin \psi \cos \beta_0,\ -g \cos \alpha_S - r \sin \beta_0) \tag{4}$$

where (r, ψ) is the source location.

r is the radial distance from rotor hub

g is the length of shaft from tilt pivot point to rotor hub

We also have

$$\vec{OS} = (x,\ y,\ z) \tag{5}$$

Combining eq (4) and eq (5), we have

$$\begin{aligned} x &= -g \sin \alpha_S - r \cos \psi \cos \beta_0 \\ y &= r \sin \psi \cos \beta_0 \\ z &= -g \cos \alpha_S - r \sin \beta_0 \end{aligned} \tag{6}$$

The component of tunnel velocity U_∞ in the direction of sound propagation $\vec{SP}$ is

$$\vec{U}_\infty \cdot \vec{SP}/|\vec{SP}| = -U_\infty (x_1 - x)/|\vec{SP}| \tag{7}$$

The effective sound speed (C_{eff}) in the direction of $\vec{SP}$ is, therefore,

$$C_{eff} = C - U_\infty (x_1 - x)/|\vec{SP}| \tag{8}$$

The time t_1 taken by the acoustical wave travelling from source S to observer P is

$$t_1 = |\vec{SP}|/C_{eff} \tag{9}$$

The time T between the $\psi = 0$ index and the acoustical waves arriving at microphone P is

$$T = \frac{\psi}{\Omega} + t_1 \tag{10}$$

where Ω is the rotor rotational speed.

Substituting eq (8) and eq(9) into eq (10), we have

$$T = \frac{\psi}{\Omega} + \frac{|\vec{SP}|^2}{C\,|\vec{SP}| + U_\infty (x - x_1)} \tag{11}$$

Since

$$|\vec{SP}|^2 = (x - x_1)^2 + (y - y_1)^2 + (z - z_1)^2 ,$$

Substituting eq (6) into the above equation, we have

$$\vec{SP}^2 = r^2 + 2r\,A(\psi) + E \tag{12}$$

where

$$A(\psi) = (-y_1 \sin\psi + g \sin\alpha_S \cos\psi + x_1 \cos\psi)\cos\beta_0 + (g\cos\alpha_S + z_1)\sin\beta_0 \tag{12a}$$

$$E = x_1^2 + y_1^2 + z_1^2 + g\,(g + 2x_1 \sin\alpha_S + 2z_1 \cos\alpha_S) \tag{12b}$$

Using eq (6), we have

$$x - x_1 = r\,B(\psi) + F \tag{13}$$

where

$$B(\psi) = -\cos\beta_0 \cos\psi \tag{13a}$$

$$F = -g \sin\alpha_S - x_1 \tag{13b}$$

substituting eq (12) and eq (13) into eq (11) we have

$$T = \frac{\psi}{w} + \frac{r^2 + 2r\,A(\psi) + E}{C\,[\,r^2 + 2r\,A(\psi) + E]^{1/2} + U_\infty\,[F + rB(\psi)]} \tag{14}$$

The speed of sound can be approximated by

$$C = 331.6 - .6073\ X\ (TEM),\ C \text{ in m/sec, TEM in } {}^{o}C$$

or

$$C = 1052 + 1.143\ X\ (TEM),\ C \text{ in ft/sec, TEM in } {}^{o}F \tag{15}$$

where TEM is the tunnel temperature.

Equation (14) is the equation used in triangulation.

T can be obtained from one microphone measurement. Coordinate (x_1, y_1, z_1) is the microphone location. a_{1S}, b_{1S}, α_S, g, TEM, and Ω all can be measured.

Equation (14) is a function of (r, ψ). Two simultaneous equations are required to solve source location (r, ψ). In other words, each microphone measurement establishes an equation (14), which represents a line on the rotor disc. This line is the intersection loci of a "collapsing sphere" (not a real sphere because of tunnel wind effect) and the blade as mentioned before. For thickness noise sources, this line represents the source region. For noise due to blade-vortex interaction or compressibility effects, the intersection point (region) of two such lines is the source location.

2.2 Numerical Procedures

For numerical calculations, eq (14) can be reduced to a fourth order algebraic equation in r with coefficients in terms of ψ and other measurable parameters.

$$r^4 + A_3(\psi) r^3 + A_2(\psi) r^2 + A_1(\psi) r + A_0(\psi) = 0 \tag{16}$$

where

$$A_0(\psi) = [E - (T - \tfrac{\psi}{\Omega})\, U_\infty F]^2 - E\,(T - \tfrac{\psi}{\Omega})^2\, C^2$$

$$A_1(\psi) = 2[2A - (T_1 - \tfrac{\psi}{\Omega})\, U_\infty B]\,[E - (T - \tfrac{\psi}{\Omega})\, U_\infty F] - 2A\,(T - \tfrac{\psi}{\Omega})^2\, C^2$$

$$A_2(\psi) = [2A - (T - \frac{\psi}{\Omega}) U_\infty B]^2 + 2[E - \frac{\psi}{\Omega}) U_\infty F]^2 - (T - \frac{\psi}{\Omega})^2 C^2$$

$$A_3(\psi) = 2[2A - (T - \frac{\psi}{\Omega}) U_\infty B]$$

For each given ψ, the four roots of r can be obtained by solving eg (16). Only real roots whose magnitude is within the span of blade are physically possible. Repeating for different ψ, the source line can be established.

Figure 2 shows a block diagram of the computational algorithm. A standard library subroutine was used in solving for the roots of eq (16). Variable step size of ψ is used to save computation time. The computer program (named INSL), which is written for a CDC 7600, is developed for the calculation of impulsive noise source and documented separately.

2.3 Sensitivity to Experimental Errors

The uncertainty of source location due to the fluctuation of rotor RPM and tunnel speed and other measurement errors are studied by perturbing the inputs to the computer program INSL. A typical rotor noise time history with its corresponding 1/rev blip is shown in Figure 3. The microphone is located straight ahead of the rotor with coordinates in meters (20.90, 0, -2.46). The noise source location changes due to perturbations on microphone location (x,y,z) are shown in Figure 4. 0.15m perturbations in three directions are made. The source lines are almost coincident for the 0.15m change in y or z direction. It

is relatively sensitive in x (i.e., streamwise) direction as shown in Figure 4. Figure 5 shows the effect of time (T) between 1/rev and microphone measurement. Time (T) is increased by .0010 sec. and decreased by .0020 sec. These correspond to the typical 0.003 sec. width of the acoustical pulse (see Figure 3). The error of .0010 sec. in T can also be translated into 2^{o} error in 1/rev blip for a rotor of 330 rpm. Typical tunnel data have a much smaller error. Figure 6 shows the effects of errors in shaft angle, tip path plane, rotor rpm, tunnel speed and temperature. One-degree errors in shaft angle and tip path plane do not significantly change the calculated source location. The effects of 2% variations in rotor rpm and tunnel speed are as shown. Source location is effected more by rotor rpm than tunnel speed. The temperature also affects the calculated source location because the speed of sound changes with temperature. The increase of $15^{o}F$ on tunnel temperature has less effect than the 2% increase in rotor rpm.

Based on the above study, we can list the parameters in the order of sensitivity as time (T) between 1/rev and acoustical pulse, rotor rpm, tunnel temperature, and tunnel speed. The tip path plane angle and shaft angle are least sensitive. The apparent source location is much more sensitive to streamwise position of the microphone than to lateral or vertical positions. Thus, for ordinary rotor tests, the experimental errors induce rather small amounts of error in noise source location.

3. Applications to Full Scale Noise Data

The triangulation technique developed in Chapter 2 will now be used to find the helicopter rotor impulsive noise source locations, based on the full scale data previously mentioned. Based on information of the source locations and rotor performance conditions, the impulsive noise mechanisms are then discussed.

3.1 Rotor Noise Data Taken by NASA/Ames

A complete set of full scale helicopter noise data were obtained by the rotor group at the Large-Scale Aerodynamics Branch, NASA Ames Research Center. A two-bladed UH-1 rotor of 48-Foot diameter was used in the experiment. It is a teetering rotor system with cyclic pitch, collective pitch and shaft tilt. Four sets of blades were tested, each set having a different tip shape. Tip shapes include thin tip, vortex diffuser tip, single swept tip and double swept tip. Detailed configurations are shown in Figure 7. The basic chord of each blade is .5334m. It should be noted that thickness distributions in the tip regions vary for the different planforms.

Six B&K microphones (five ½-inch and one 1-inch) with noise cones were used in the measurements. The microphone locations are shown in Figure 8, and the coordinates of the microphones are listed in Table 1.

The microphone data and 1/rev azimuth blip index were recorded simultaneously on a 14-track Ampex 1300A analog magnetic tape recorder. The tape speed was 30 ips, and the center frequency (FM) was 108 kHz.

The frequency response is up to 20 kHz. The acoustical data were also digitally processed and filtered for the frequency passband of 75 Hz to 500 Hz. The digital filtering makes use of Chebyshev filters to obtain phase free and distortionless data. Figure 9 shows the comparison of raw and filtered rotor acoustical time history. The impulsive noise waveform of the filtered data is the same as that of the raw data (for triangulation purposes), but the filtered wave form is more readily identified. The bandpass filtering process eliminated tunnel background noise and the low frequency rotational noise due to mean thrust and drag at the low frequency end, as well as rotor broadband noise and some tunnel noise at the high frequency end.

3.2 Noise Source Locations and Noise Mechanisms

The following operating conditions are under study:

$C_T/\sigma = .08$, $\mu = .3$, $M_{t,90} = .95$, $\Omega = 34.56$ rad/sec and

$U_\infty = 74.59$ m/sec.

The acoustical time histories as measured by different microphones are shown in Figures 10 through 13. The microphone numbers are those referred to in Figure 8. The measurements of mic 1 and mic 5 have not been shown because they are similar to those of mic 2 shown in Figure 11. The data of thin tip, single swept tip, double swept tip, and vortex diffuser tip rotors are presented in each figure. The general waveforms are characterized by two pulses per revolution. The arrow on each figure indicates the acoustical pulse which is generated by the

advancing blade. The small pulses between two large pulses are believed to be the reflections from wind tunnel surfaces or other unrelated noise. Due to the large distance between rotor and surrounding surfaces, the incident pulses can be identified readily. The 1/rev blips which are generated at $\psi = 0$ are shown in each figure.

Note that the acoustical pulse as measured at mic 3 is a negative pulse, followed by a sharp increasing of acoustical pressure. The waveforms are similar for different blade tips. The occuring time is independent of tip shapes. These saw tooth-like waveforms were also observed in the in-flight experiment[19]. In contrast to these results, positive pulses are measured by Microphones 2, 4, and 6. The waveforms of these positive pulses are quite different for different sets of blades, in addition to the different occuring times. Based on these observations, one may suspect that the acoustical sources measured by mic 3 are different from those by mics 2, 4 and 6. The waveform measured at mic 2 are very similar to that at mic 6, although with different amplitude. This indicates mic 2 and mic 6 may be measuring the acoustical pulse generated from one source. The detail waveform of mic 4 measurement is different from those of mics 2 and 6, but with the same general characteristics. These indicate that mic 4 measures the same mechanism as in mics 2 and 6, but at different locations. The triangulation results support these observations.

Figure 14 shows the results of the triangulation calculations. Six curves are shown, corresponding to the peaks of the acoustical pulses measured by six microphones. Each one, therefore, corresponds to a possible acoustical source line.

The source lines of mic 1, 3 and 5 are located in the second quadrant. The impulsive noise measured at mics 1, 3 and 5 are believed to be thickness noise. The reasons are: (1) the pressure pulse is negative; (2) the source lines are located in the second quadrant; (3) the source lines do not intersect each other; (4) the amplitude of pulse is independent of C_T/σ. Thickness noise is due to the accumulation of acoustical pressures which are generated from different portions of rotor disc but reach the observer at the same time. This is purely an acoustic effect. They will not intersect each other. Another possibility for source lines not crossing each other is where different microphones measure different sources. Since the microphones are so close to each other, it is virtually impossible to have aerodynamic sources of such a narrow acoustical directivity. Thus, these pulses are probably thickness noise. Thickness noise is highly dependent on local Mach number. Only the outer portion of the blade (typically 25%) are generating significant thickness noise as indicated in ref. (21).

Since the acoustical pulses have a finite width, their corresponding sources are actually regions instead of lines. Figure 15 shows the source regions of thickness noise. The source regions of mic 1 and mic 3 are in the second quadrant. The source region of mic 5 is on the advancing side of the rotor disk.

The source lines of mic 2 and mic 6 in Figure 14 intersect each other at $\psi = 54^{o}$. This indicates an aerodynamic source at this region. The noise mechanism is due to blade-vortex interaction. Referring to Figure 16, the geometry of a rotor rigid wake indicates the advancing blade intersects with preceding vortex near $\psi = 58^{o}$. This is very close to the result of triangulation, considering the crude rigid wake model.

The source line of mic 4 extends from $\psi = 24^{o}$ to $\psi = 35^{o}$. Figure 16 shows the blade interacts with its own vortex of one revolution old, at $\psi = 45^{o}$. This discrepancy between triangulation and rigid wake geometry is believed due to wake distortion. Recently, a Laser Velocimeter (LV) measurement of rotor wake[22] has been done in NASA Ames Research Center. Results show the tip vortex geometry is very close to rigid wake before the influence of next blade. However, the vortex wake is distorted considerably by the passing blade. Rigid wake geometry is no longer valid. The triangulation does indicate a large distortion of vortex wake.

The details of the noise production by the source at $\psi = 35^{o}$ and $\psi = 54^{o}$ are quite different, although both are due to blade-vortex interaction. The one at $\psi = 35^{o}$ is of two-dimensional type interaction, because it can be modeled as a wing of infinite span translating through the still air and interacting with an infinite vortex filament[3,15]. The magnitude and spanwise distribution of the blade loading is steady (frozen). The effective traveling Mach Number (Me) of the blade does not exceed one, but the convective Mach Number (Mc) of the loading

through the fluid can be greater than one. Derived in reference (3), Mc = Me/sin Λ where Λ is the angle between blade and vortex filament. The convective Mach number Mc can be easily greater than one when Λ is small. The basic mechanism for the generation of impulsive is due to the convection of a frozen force distribution through the air with a supersonic Mach number. A large portion of the blade span is involved in the noise generation.

The noise source at $\psi = 54^{o}$ is due to a three dimensional phenomenon which occurs near the blade tip. The blade Mach number (Me) is high, but the interaction angle is also quite large so that the loading convection is subsonic. It is not an efficient noise generator for a "steady" loading convecting at a subsonic speed. Since the blade-vortex interaction begins at the tip region, both the lift magnitude and its spanwise distribution vary significantly with time. It is this "unsteadiness" which generates the impulsive noise.

4. Conclusions

Based on full scale rotor noise data measured at NASA Ames Research Center, triangulation results show there exist at least three different noise sources. The sources of thickness noise which are purely due to acoustical effects are found to be located in the second quadrant and advancing side of rotor disk. Two aerodynamic sources are found in the first quadrant. One is due to a blade interacting with the vortex of the preceding blade. The other source is due to a blade interacting with its own vortex from the previous revolution.

The triangulation technique developed in this program is very useful in locating the impulsive noise source and consequently understanding noise mechanisms. This technique is rather insensitive to experimental errors of standard rotor tests. It gives accurate results and can be used for studying thickness noise. A once-per-rev blip is used as a time reference. This is different from other triangulation techniques which use the time difference between microphones.

The next step would be to develop an on-line triangulation including acoustical data acquisition, processing and analysis. This can be done by utilizing the existing DAS data system at NASA Ames Research Center. The on-line triangulation has several advantages. Any acoustical effects due to the change of rotor design or operating conditions can be discovered while the experiments are taking place. Any change of test plans can be decided quickly, based on these results. Flow measurements, such as with an LV can then be restricted to the known source

region. A lot of manpower, tunnel time and cost can thus be saved by implementing an online triangulation technique such as described above.

REFERENCES

1. Cox, C. R.: Aerodynamic Sources of Rotor Noise. J. of the Am. Hel. Soc., January 1973.

2. Ham, N. D.: Some Preliminary Results from an Investigation of Blade Vortex Interaction. J. of the Am. Hel. Soc., 19(2), 1974.

3. Widnall, S. E.: Helicopter Noise Due to Blade-Vortex Interaction. J. of Acoustical Soc. of Am., 50, 354-365, 1971.

4. Filotas, L. T.: Vortex Induced Helicopter Blade Loads and Noise. J. of Sound and Vibration, 27, 3, 387-398, 1973.

5. Chu, S. and Widnall, S. E.: Lifting-Surface Theory for a Semi-Infinite Wing in Oblique Gust. AIAA Journal 12, 12, 1672-1678, December 1974.

6. Arndt, R. A. and Borgman, D. C.: Noise Radiation from Helicopter Rotors Operating at High Tip Mach Number. 26th Annual National Forum, the American Helicopter Society, June 1970.

7. Lyon, R. H.: Radiation of Sound by Airfoils that Accelerate near the Speed of Sound. J. Acoustical Soc. Am., 49, 894-905, 1971.

8. Lyon, R. H.; Mark, W. D.; and Pyle, R. W., Jr.: Synthesis of Helicopter Rotor Tips for Less Noise. Proceedings, Helicopter Noise Symposium, ARO-Durham, September 28-30, 1971.

9. Ffowcs Williams, J. E. and Hawkings, D. L.: Sound Generation by Turbulence and Surfaces in Arbitrary Motion. Phil. Trans. of the Royal Soc. of London (A), 264, 321-342, 1969.

10. Lighthill, M. J.: On Sound Generated Aerodynamically, I General Theory. Proc. of Royal Society (A), 221, 564-587, 1952.

11. Curl, N.: The Influence of Solid Boundaries upon Aerodynamic Sound. Proc. of Royal Society (A), 231, 505-514, 1955.

12. Farassat, F; Pegg, R. J.; and Hilton, D. A.: Thickness Noise of Helicopter Rotors at High Tip Speeds. AIAA Paper No. 75-453, AIAA 2nd Aero-Acoustics Conference, Hampton, Virginia, March 24-26, 1975.

13. Riedel, S. C. and Schairer, J. D.: Acoustic Data Obtained from Blade-Vortex Interaction Study. Verto. Interoffice Mem., The Boeing Co., Vertol Division, June 1970.

14. Surrendraiah, M.: An Experimental Study of Rotor Blade-Vortex Interaction. Pennsylvania State University, NASA CR-1573, May 1970.

15. Widnall, S. E.; Chu, S.; and Lee, A.: Theoretical and Experimental Studies of Helicopter Noise due to Blade-Vortex Interaction. Proceedings, Helicopter Noise Symposium, ARO-Durham, September 28-30, 1971.

16. Bausch, W. E. and Schlegel, R. G.: An Experimental Study of Helicopter Rotor Impulsive Noise. Proceedings, Helicopter Noise Symposium, ARO-Durham, September 28-30, 1971.

17. Widnall, S. E.; Lee, A.; and Bauer, P.: Experimental Results of Rotational Noise in Forward Flight. Proceedings, American Helicopter Society, Mideast Region Symposium, Essington, Pennsylvania, October 1972.

18. Charles, B. D.: Acoustic Effects of Rotor-Wake Interaction During Low-Power Descent. Proceedings, American Helicopter Society Symposium on Helicopter Aerodynamic Efficiency, March 6-7, 1975.

19. Schmitz, F. H. and Boxwell, D. A.: In-Flight Far-Field Measurement of Helicopter Impulsive Noise. 32nd Annual Forum of American Helicopter Society, Washington, D. C., May 1976.

20. Vause, C. R.; Schmitz, F. H.; and Boxwell, D. A.: High Speed Helicopter Impulsive Noise. 32nd Annual Forum of American Helicopter Society, Washington, D. C., May 1976.

21. Farassat, F.: Theory of Noise Generation from Moving Bodies with an Application to Helicopter Rotors. NASA TR R-451, 1975.

22. Biggers, J. C.; Lee, A.; Orloff, K. L.; and Lemmer, O. J.: Measurements of Helicopter Rotor Tip Vortices. 33rd Annual Forum of American Helicopter Society, Washington, D. C., May 1977.

Table 1 The Coordinates of Microphones
(refer to Figure 1 for coordinate system)

Mic No. (See Figure 8)	X (ft)	X (m)	Y (ft)	Y (m)	Z (ft)	Z (m)
1	68.24	20.80	-20	6.096	8.06	2.457
2	6.99	2.131	5	1.524	1.25	.3810
3	68.58	20.90	0	0	8.07	2.460
4	-13.84	-4.215	10.92	3.328	-1.08	.3292
5	68.83	20.98	20	6.096	8.08	2.463
6	12.41	3.783	12.83	3.911	+7	2.134

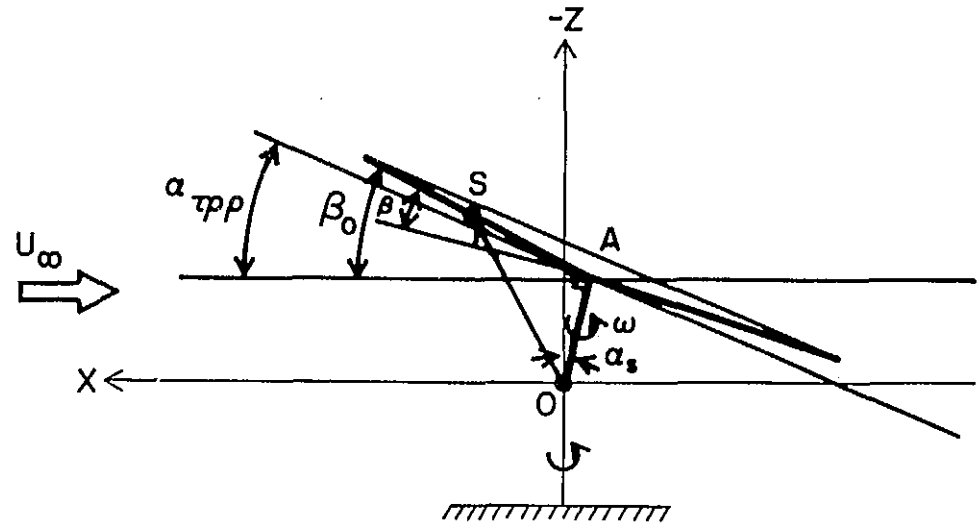

(a)

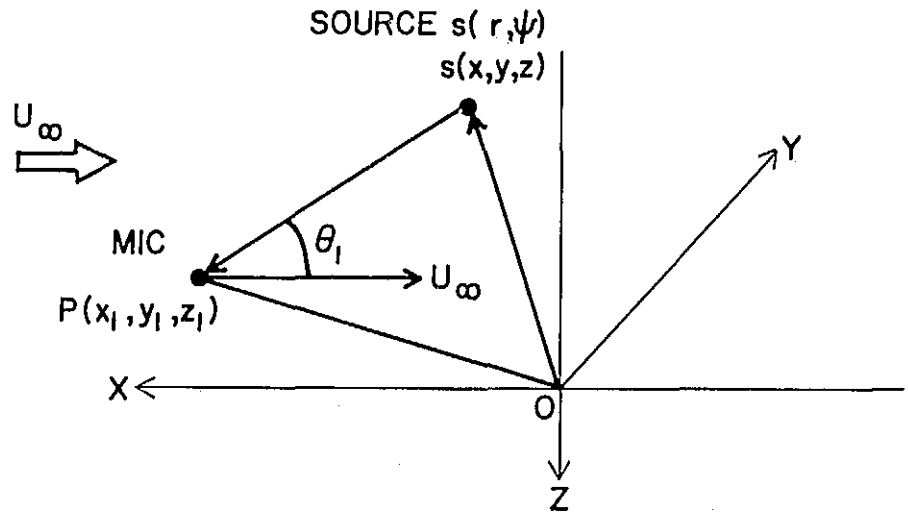

(b)

FIGURE 1.- DEFINITION OF COORDINATES

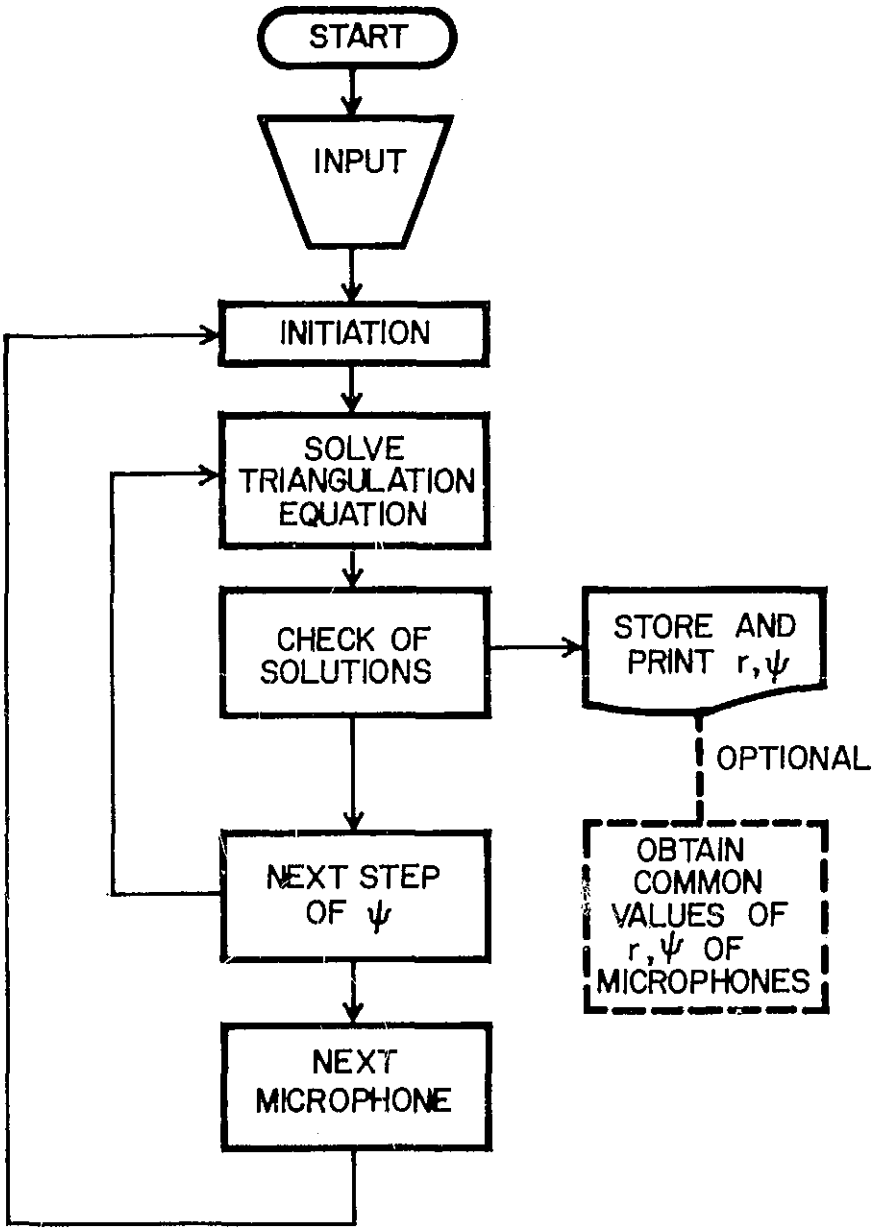

FIGURE 2.- BLOCK DIAGRAM

Ω = 330 RPM

U = 146.3 KNOTS = 75.26 m/sec

$\alpha_S = \alpha_{T\rho\rho} = -5°$

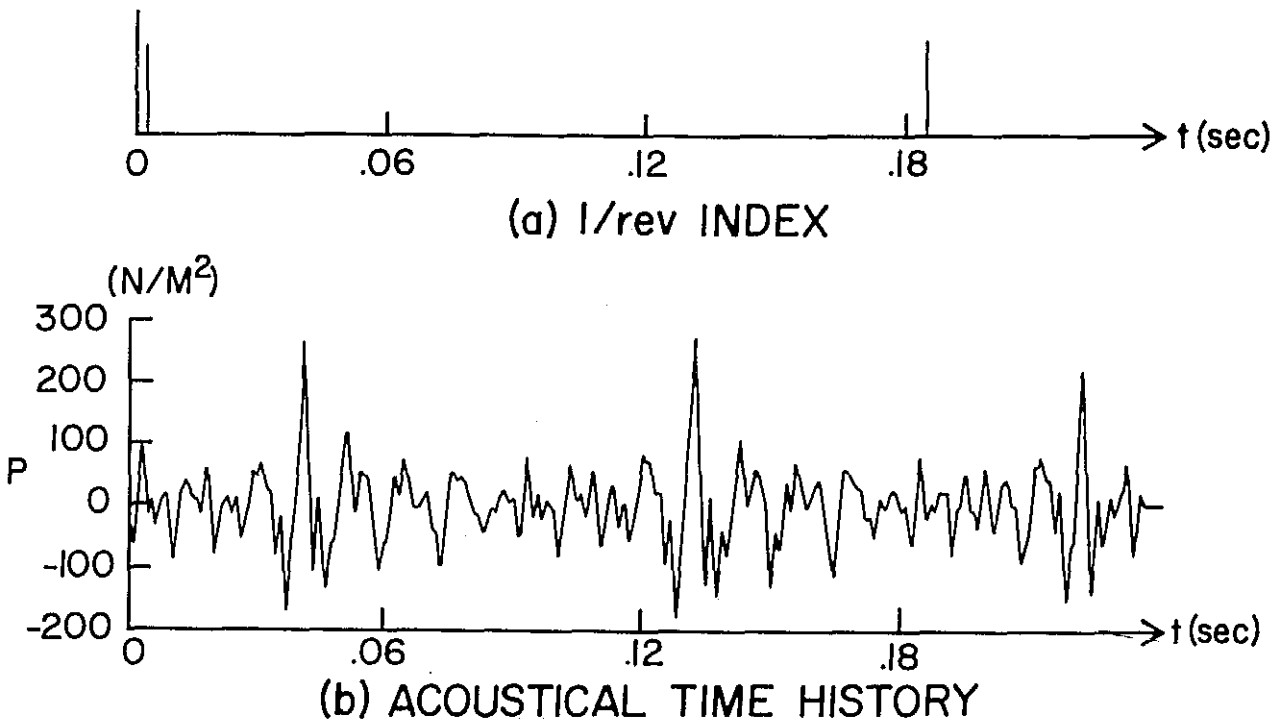

FIGURE 3.- A TYPICAL HIGH SPEED ROTOR NOISE TIME HISTORY (FILTERED) OBTAINED IN THE 40- BY 80-FOOT WIND TUNNEL, NASA AMES RESEARCH CENTER

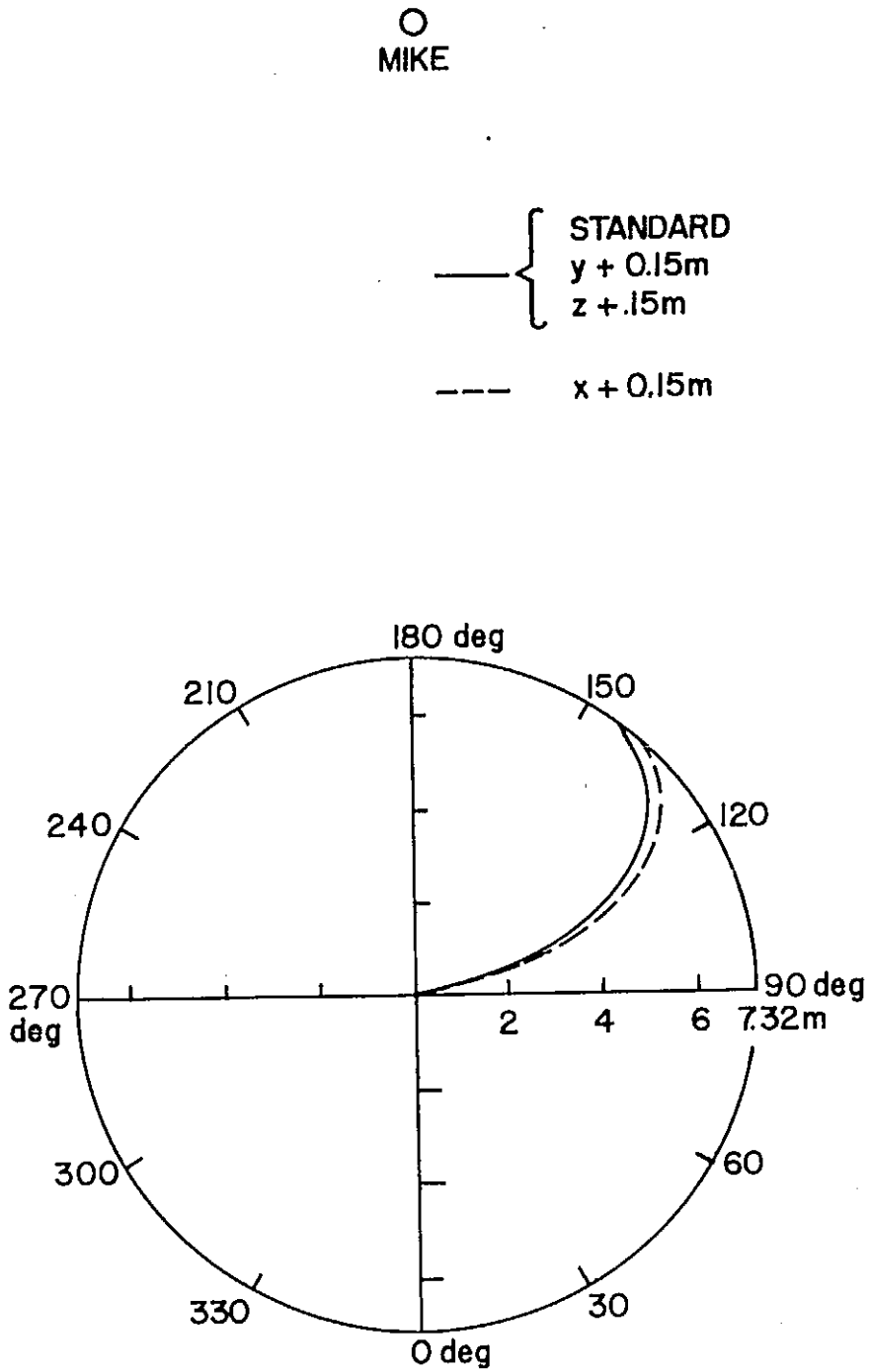

FIGURE 4.- THE EFFECT OF MICROPHONE LOCATION ON APPARENT SOURCE LOCATIONS

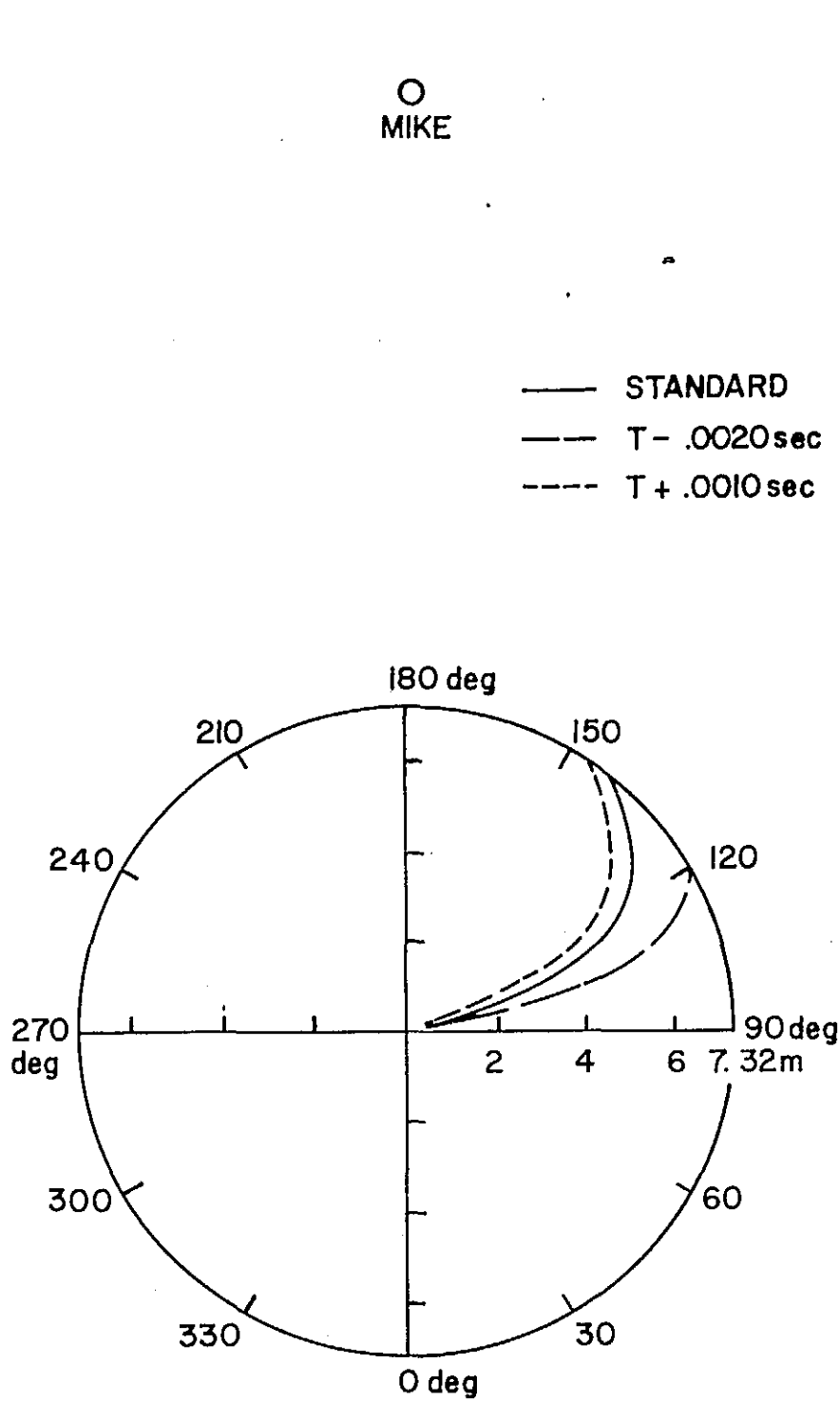

FIGURE 5.- THE EFFECT OF TIME BETWEEN 1/REV INDEX AND ACOUSTICAL PULSE ON APPARENT SOURCE LOCATIONS

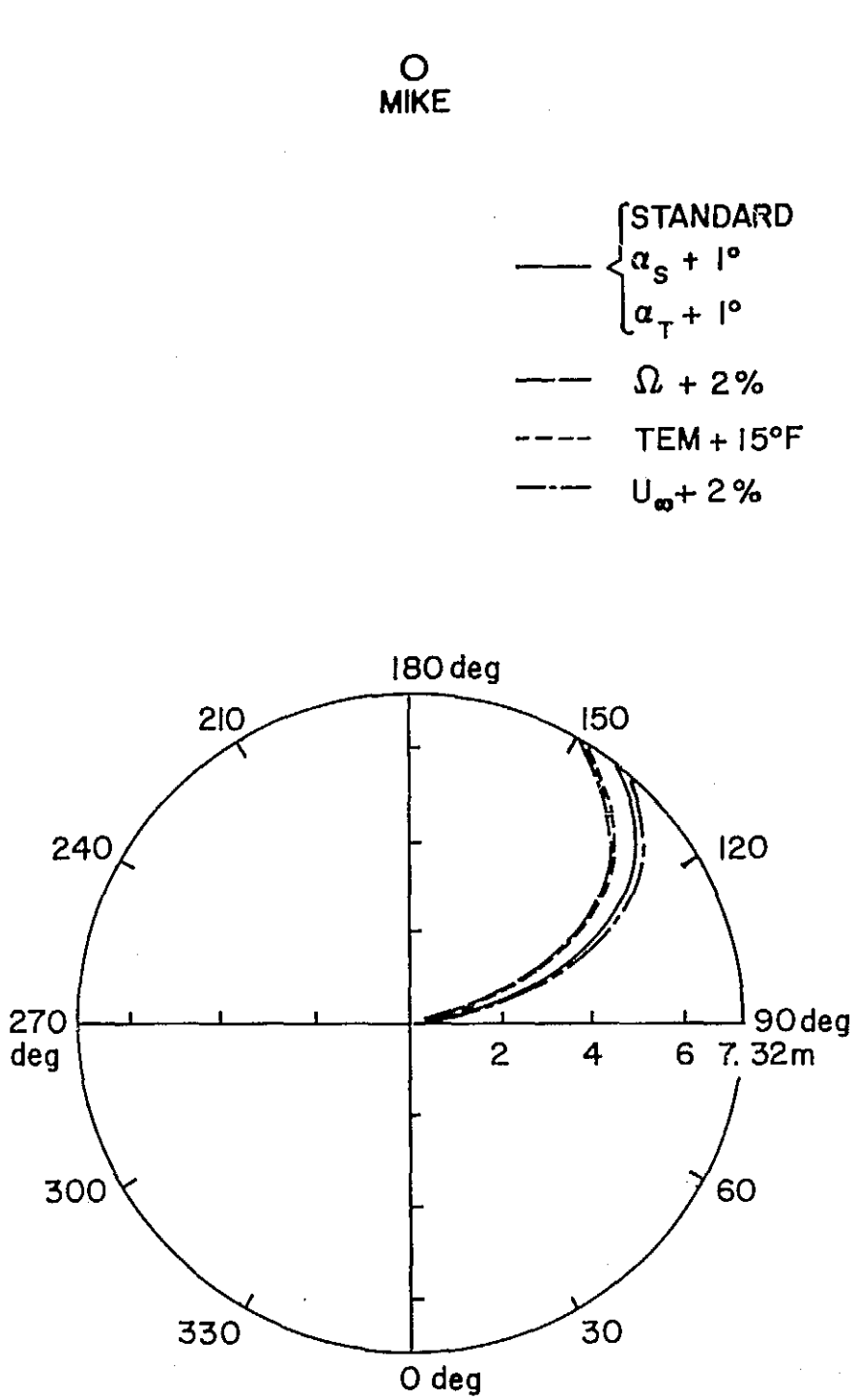

FIGURE 6.- THE EFFECT OF SHAFT ANGLE, TIP PATH PLANE, ROTOR RPM, TUNNEL SPEED AND TEMPERATURE ON APPARENT SOURCE LOCATIONS

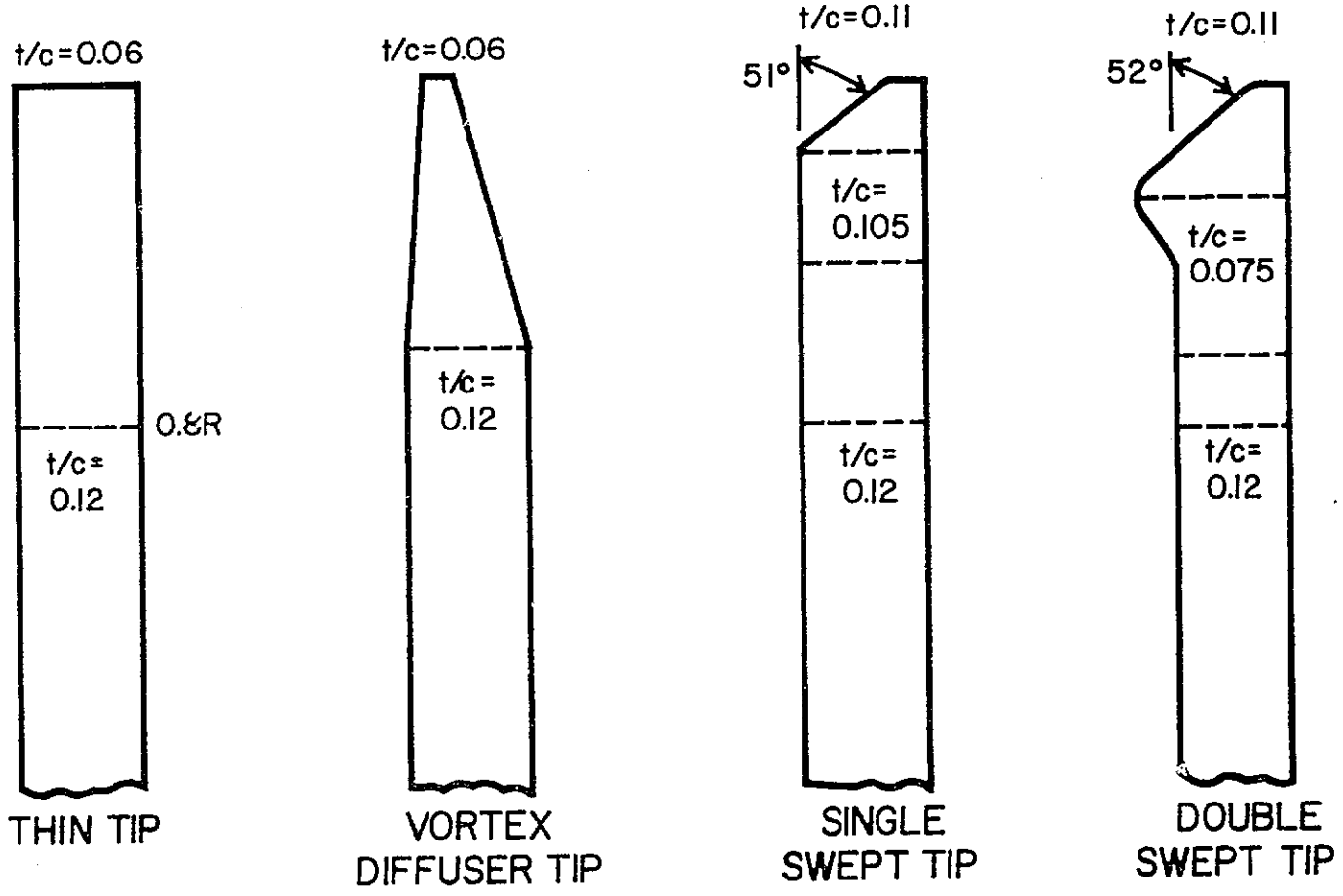

FIGURE 7.- UH-1 TIP SHAPES

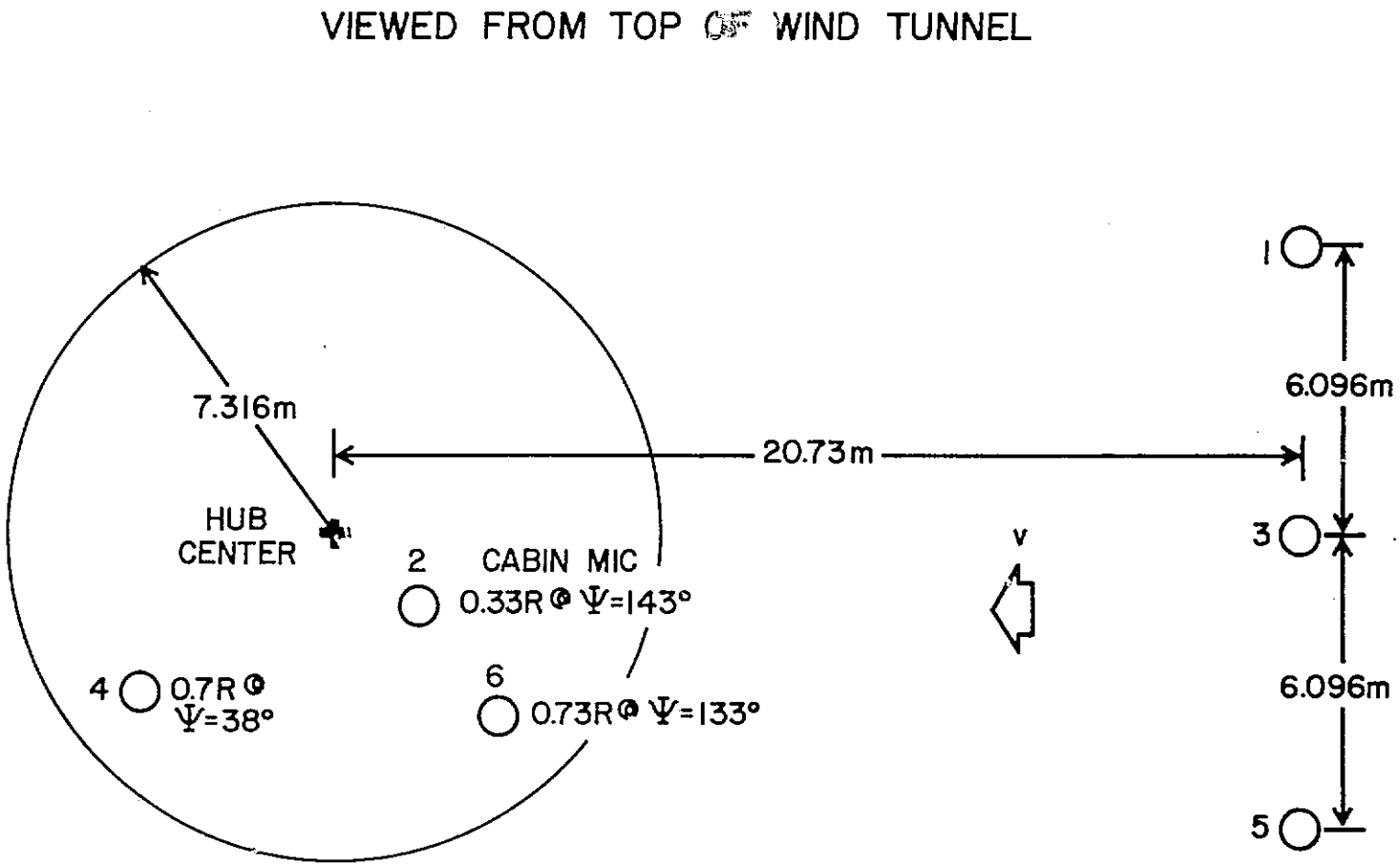

FIGURE 8.- MICROPHONE LOCATIONS

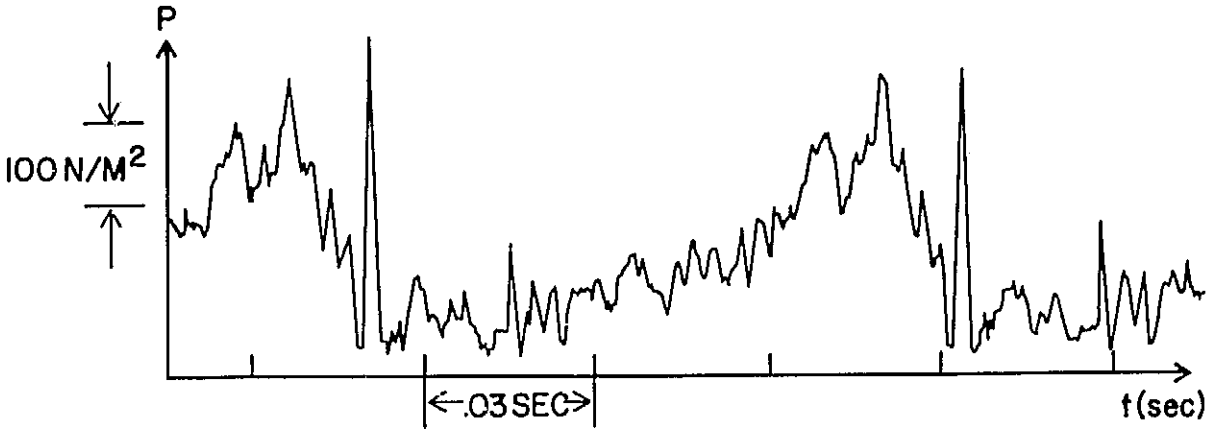

(a) RAW DATA

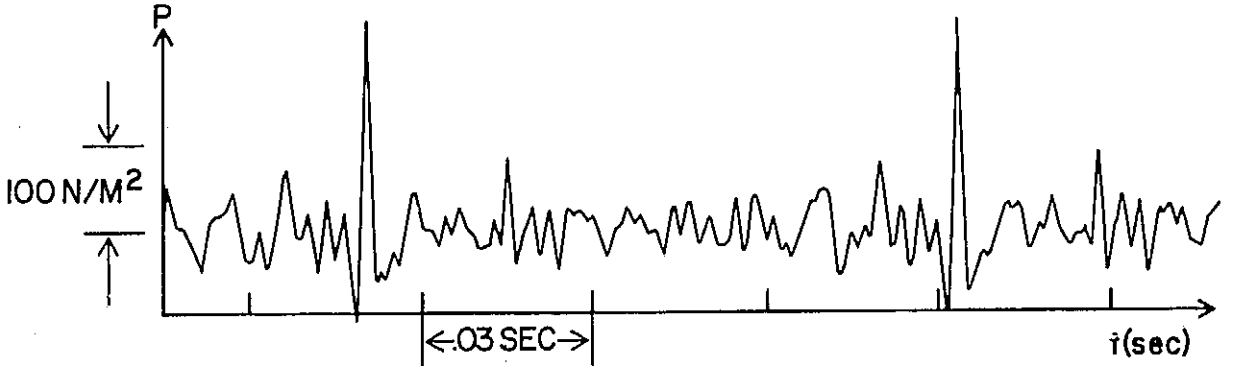

(b) DIGITALLY FILTERED DATA

FIGURE 9.- TYPICAL ROTOR NOISE TIME HISTORY, RAW DATA AND DIGITALLY FILTERED DATA

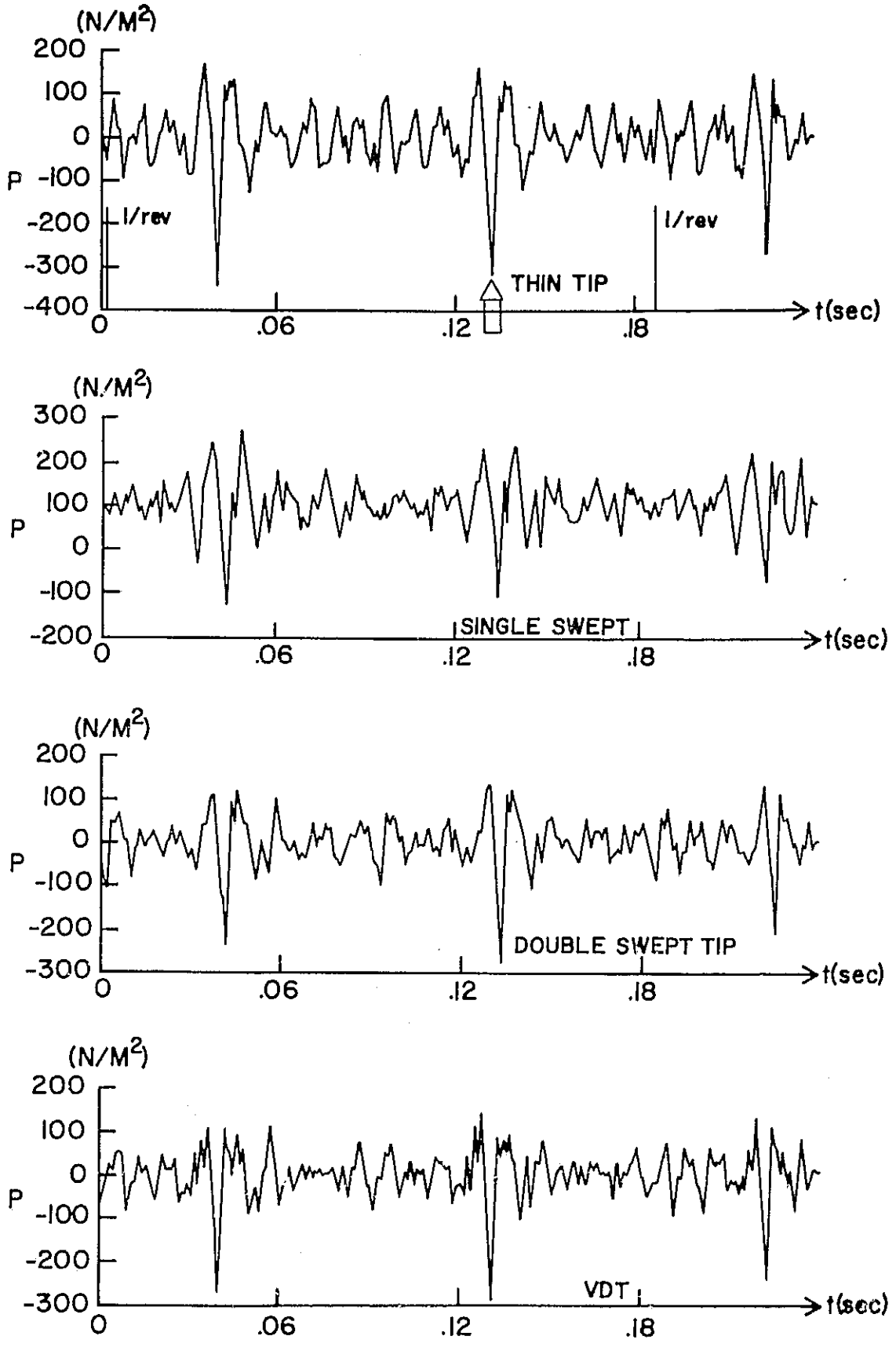

FIGURE 10.- ROTOR ACOUSTICAL TIME HISTORY AS MEASURED BY MIC 3

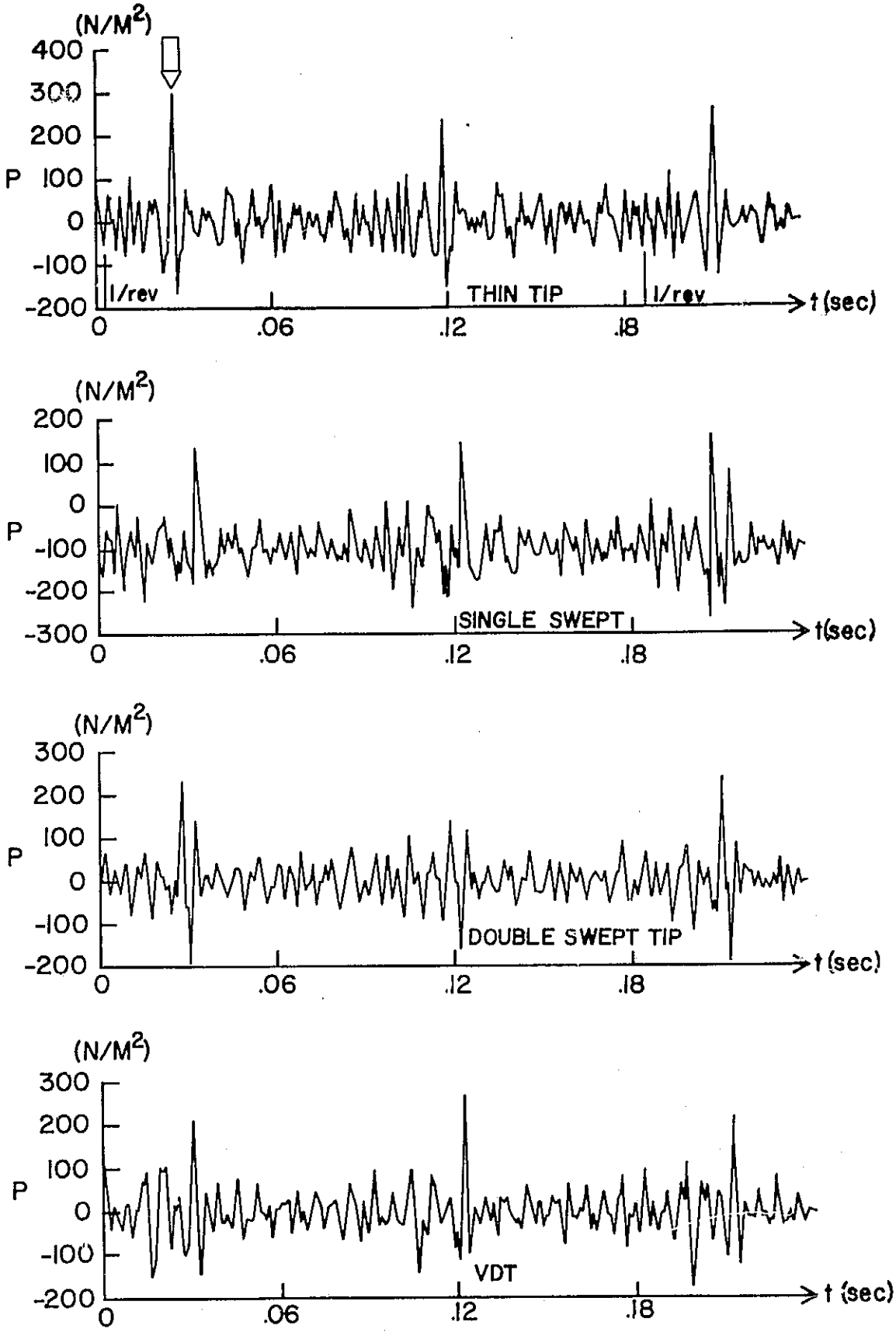

FIGURE 11.- ROTOR ACOUSTICAL TIME HISTORY AS MEASURED BY MIC 4

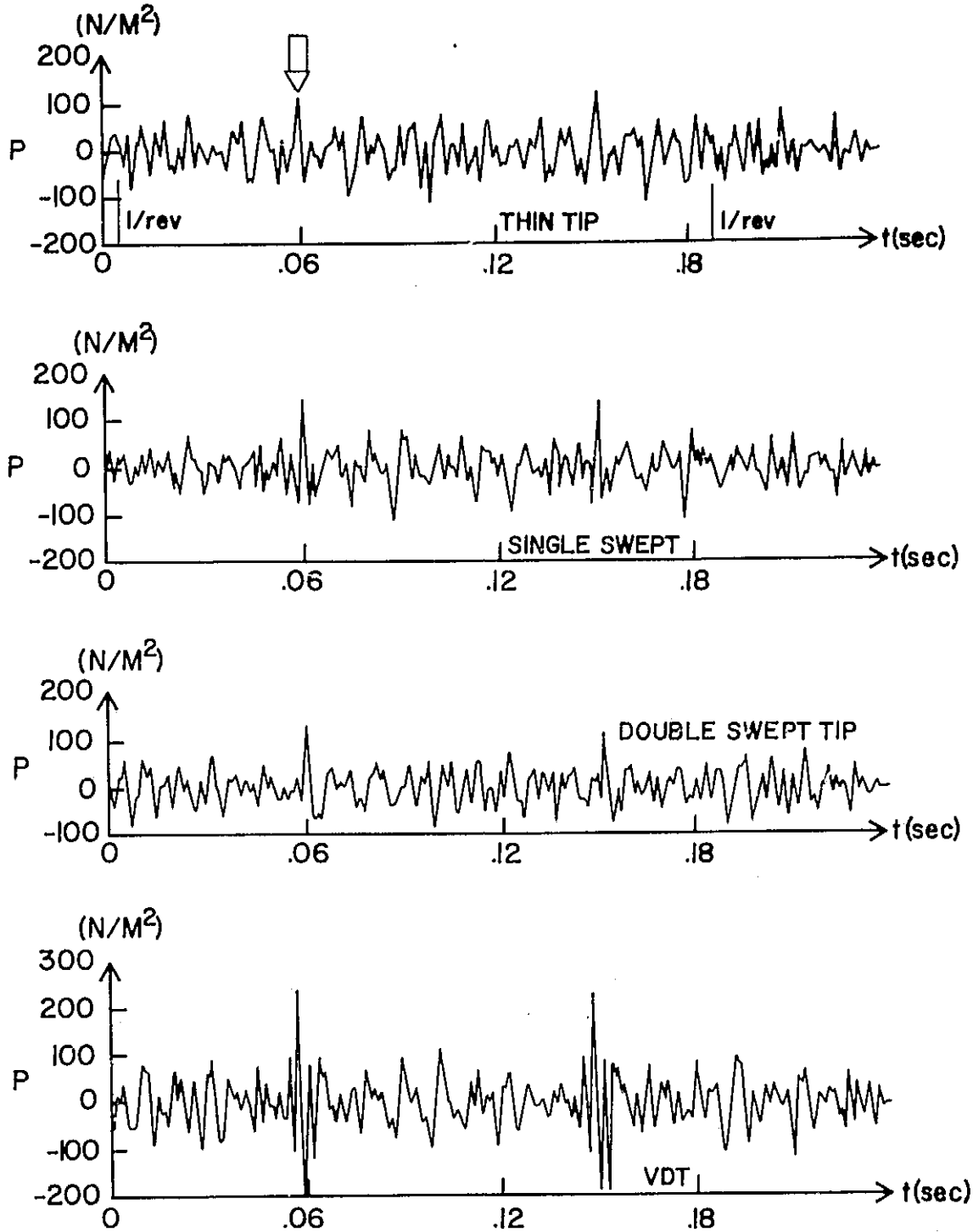

FIGURE 12.- ROTOR ACOUSTICAL TIME HISTORY AS MEASURED BY MIC 2

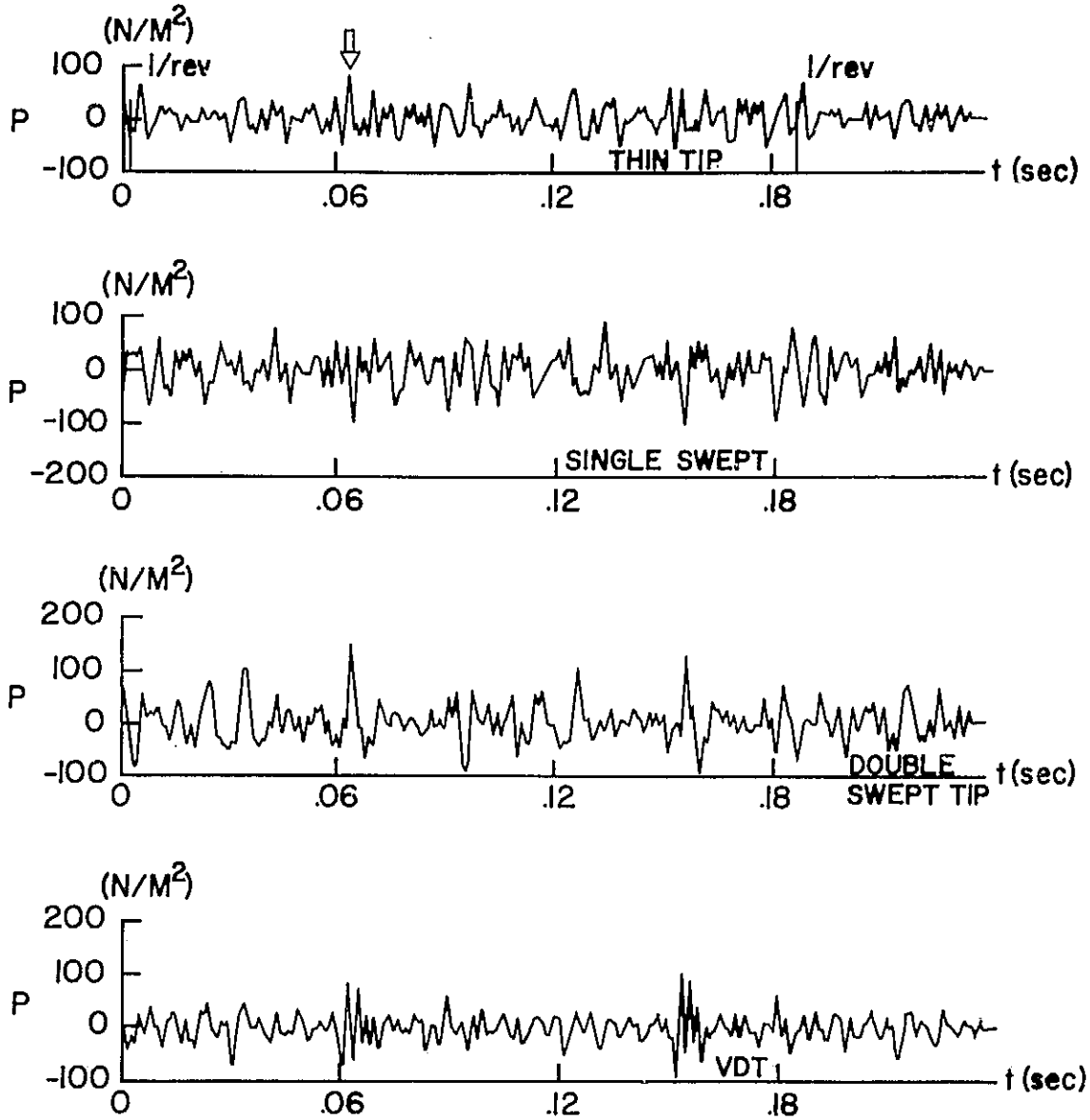

FIGURE 13.- ROTOR ACOUSTICAL TIME HISTORY AS MEASURED BY MIC 6

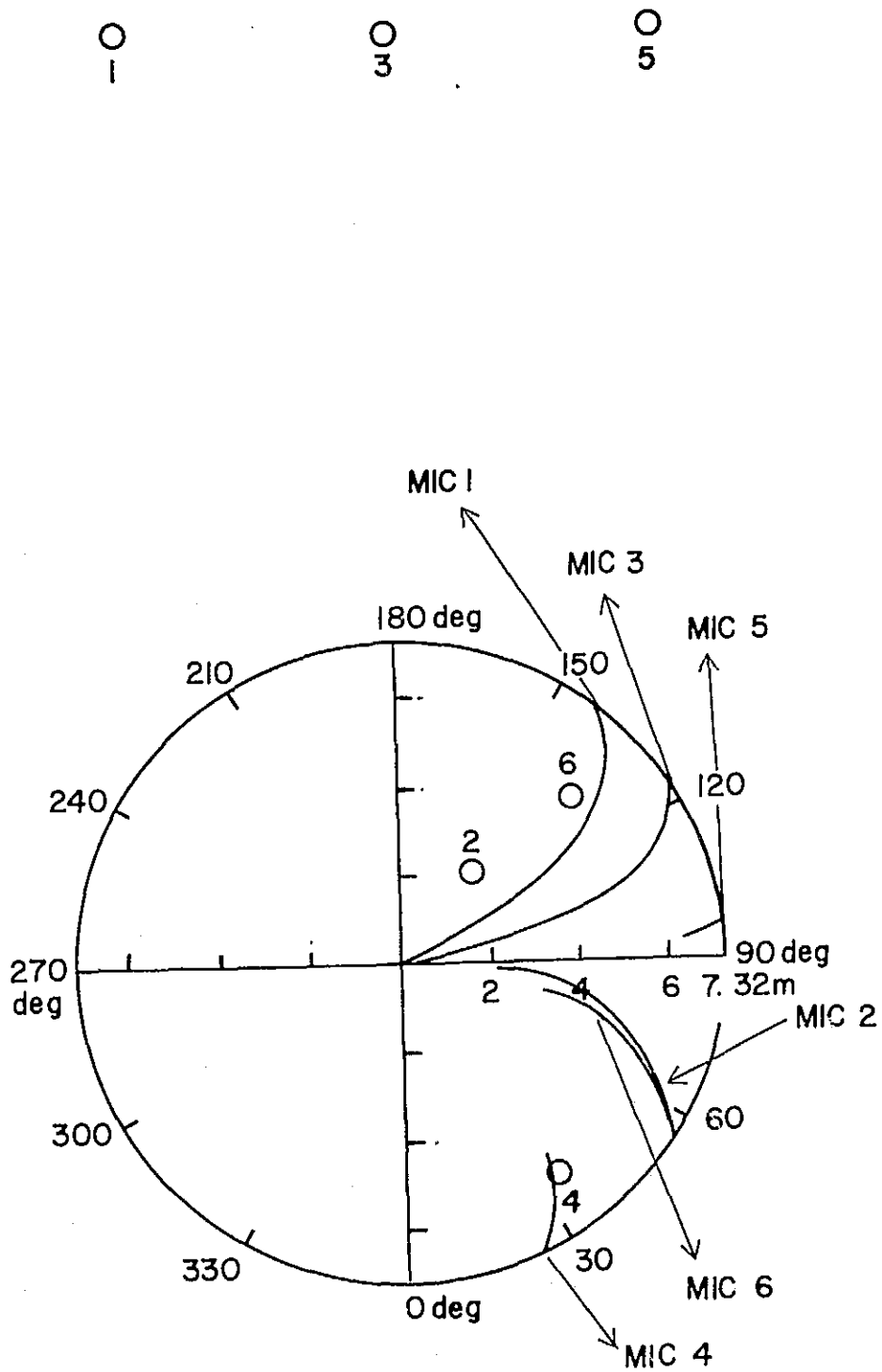

FIGURE 14.- RESULTS OF ACOUSTICAL TRIANGULATION

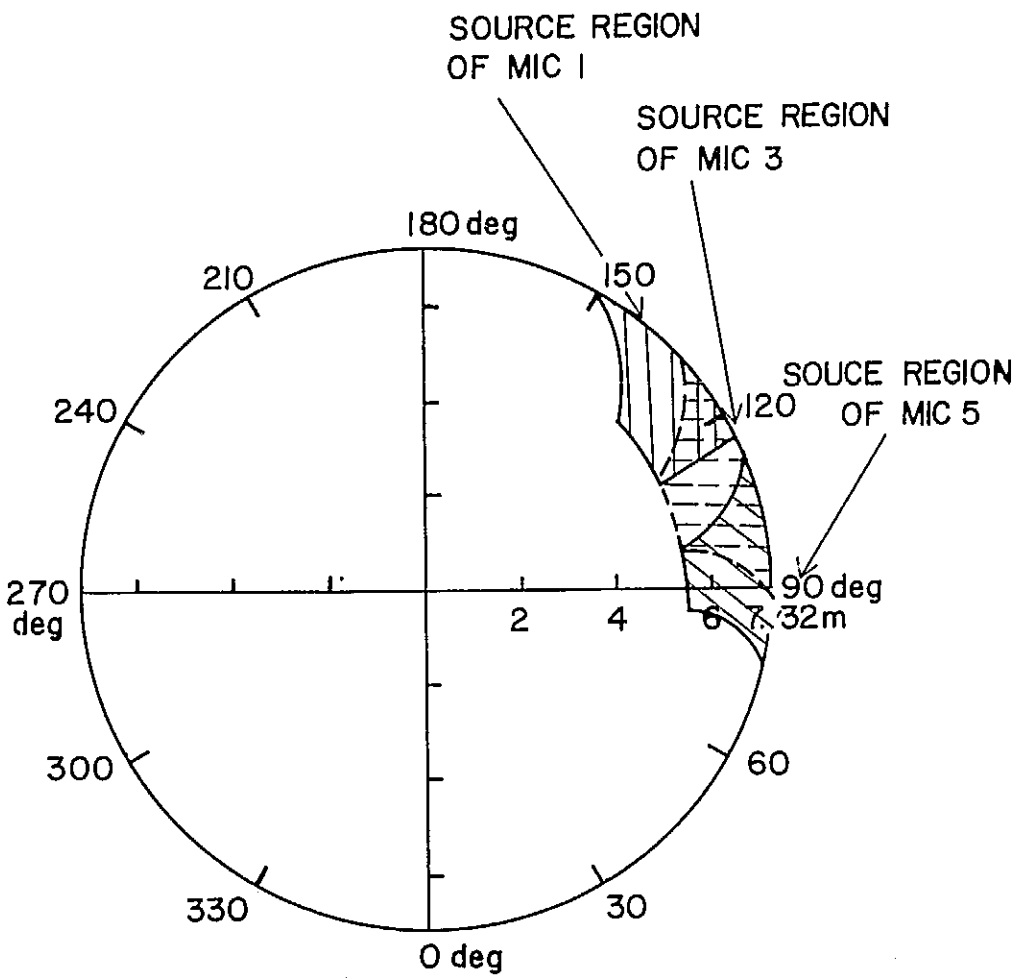

FIGURE 15.- SOURCE REGIONS OF THICKNESS NOISE

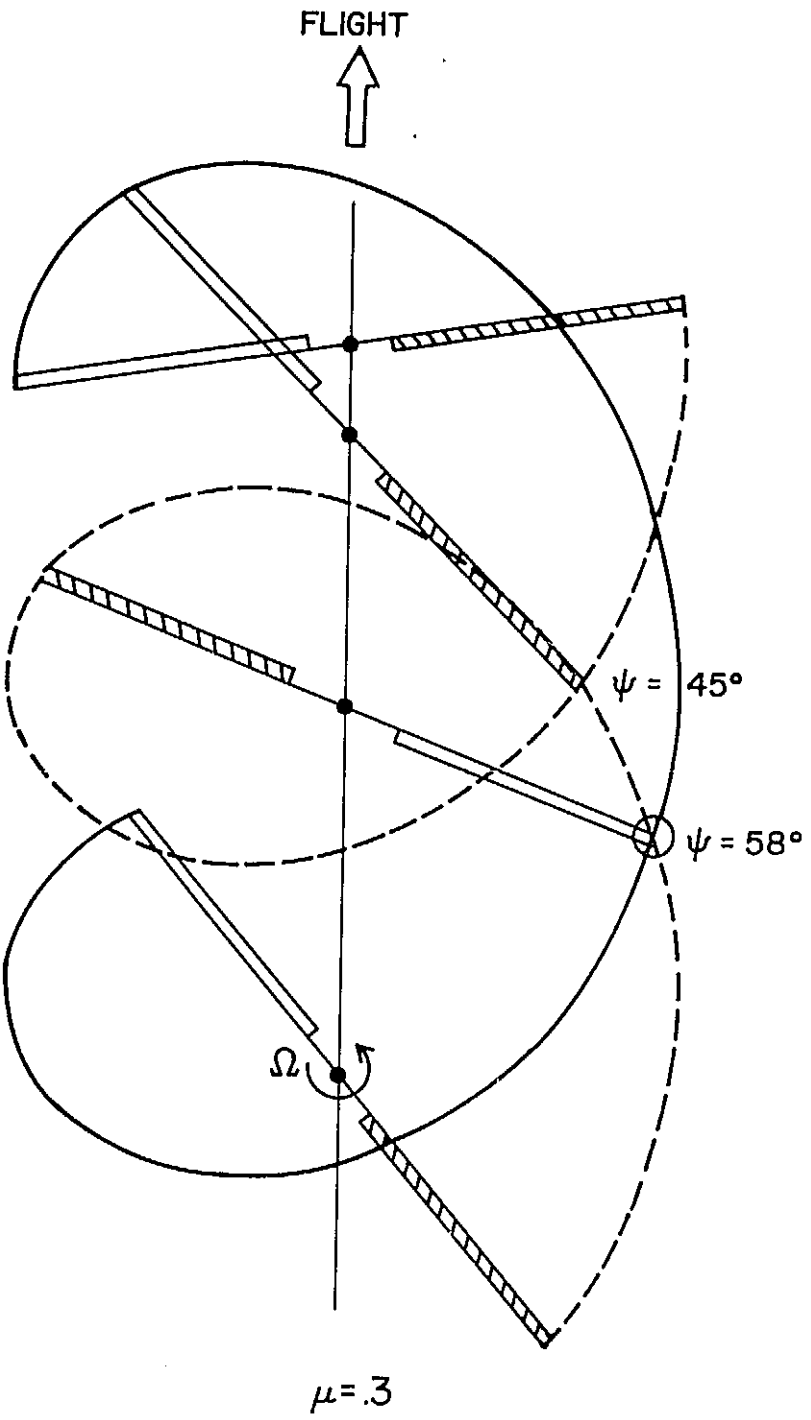

FIGURE 16.- THE GEOMETRY OF ROTOR RIGID WAKE